THE PRE-FLIGHT CALIBRATION OF THE ISOPHOT INSTRUMENT

D. Lemke[1], U. Grözinger[1], B. Schulz[1,2], J. Wolf[1,3], U. Klaas[1], I. Rasmussen[4] and F. Garzón[5]

[1]Max-Planck-Institut für Astronomie, Heidelberg, Germany
[2]ISO Data Centre, European Space Agency, Villafranca del Castillo, P.O. Box 50727, 28080 Madrid, Spain
[3]NASA Ames Research Center MS T3B, Moffet Field, CA 94035-1000, USA
[4]Danish Space Research Institute, Copenhagen, Denmark
[5]Instituto de Astrofisica de Canarias, Tenerife, Spain

ABSTRACT

Extensive characterisation of subsystems such as detectors and their curing, preamplifiers, filters, on-board secondary standard sources and cryomechanisms were the basis for the understanding of the assembled instrument and the development of a dedicated CALibration FACility for ISOPHOT. In the CALFAC the instrument was fully calibrated and the Astronomical Observing Templates tested. The high reproducibility of measurements was confirmed. This allowed the in-flight performance to be predicted to within a factor of 2. The operation of replica detectors and the stand-by of an operational flight spare unit after the flight model delivery allowed the development of countermeasures for a few non-ideal properties prior to launch and during the mission.

Key words: Instrumentation: detectors – Instrumentation: photometers – Space vehicles: instruments – Infrared: general

1. THE GOALS

Planned as a versatile photometric instrument for ESA's Infrared Space Observatory, the ISOPHOT instrument introduced various new components into a cold space experiment: several large filter wheels, stressed Ge:Ga detectors, integrating capacitive trans-impedance CMOS preamplifiers, to mention only the most important ones (Lemke et al. 1993a, Lemke et al. 1993b). In order to cover the broad wavelength range from 2.5 to 240 μm, four different detector types had to be applied. It is therefore obvious that the "preflight calibration" of such a novel and complex instrument had to start with a thorough characterisation of its properties and behaviour under varying conditions. Only after having gained this insight could we start the calibration proper: correlating the signals from ISOPHOT (Vs^{-1} of the integrating amplifiers) to the incident flux of the standard source (in Jy or MJy sr^{-1}). Ideally, this relation should be established for all times in the future with changing operational conditions and flux prehistories. The basic planning for the preflight activities involved five steps:

1. Simulation of ISO's environment (cryo-vacuum, low temperatures and low photon background, telescope beam, high energy particle flux, etc.).
2. Simulation of celestial targets/standards by a Black Body Source.
3. Setting of instrumental parameters (bias voltages, detector temperatures, cold electronics supplies, etc.) to optimal values for the large incident flux range (10^{-17} – 10^{-12} W).
4. Calibration of instrument internal secondary standard sources for a wide flux range.
5. Development of procedures for in-orbit performance verification and curing of temporal radiation damage of the detectors.

When planning these procedures we had to remember several additional requirements known beforehand and others emerging during the development phase in the early 90ies: (i) no end-to-end calibration was planned with ISO, therefore the telescope, the beam splitting optics and baffles were not included in the calibration, (ii) the in-flight conditions such as detector temperatures and photon background were only approximately known, (iii) there was concern that self-emission within ISO and bright celestial sources might produce straylight in ISOPHOT's long wavelength channels, (iv) we had to simulate ISO's daily passage through the Earth's radiation belts and knew that for safety reasons this simulation would be impossible in a larger calibration facility, (v) two separate instruments (FM and FS) had to be characterised and calibrated sequentially with limited resources, both in personnel and funds and finally (vi) there were changing schedules for the instrument delivery dates. The above mentioned factors made it impossible to go for a full and final calibration of the instruments on ground in a calibration facility. We therefore took a practical approach stepping up the learning curve by:

– an extensive instrument subsystem characterisation in the MPIA infrared laboratories (Figure 1), followed by
– the full instrument level calibration in a specially developed Calibration Facility in the clean room of the industrial prime contractor DORNIER (Figure 2).

2. SUBSYSTEM CHARACTERISATION AT MPIA

Most of the laboratory effort was devoted to studying the responsivity, noise and dark current of the different detector materials under varying temperature and background conditions and as a function of the bias voltages (Grözinger et al. 1993). The signal transient times and the tendency to spontaneous spiking were also considerations. This led to the selection of optimal operational conditions, such as the inclusion of heaters

Proceedings of the Conference "The Calibration Legacy of the ISO Mission", VilSpa, Spain, February 2001
ESA SP-481, 2003, eds. L. Metcalfe, A. Salama, S. B. Peschke & M. F. Kessler

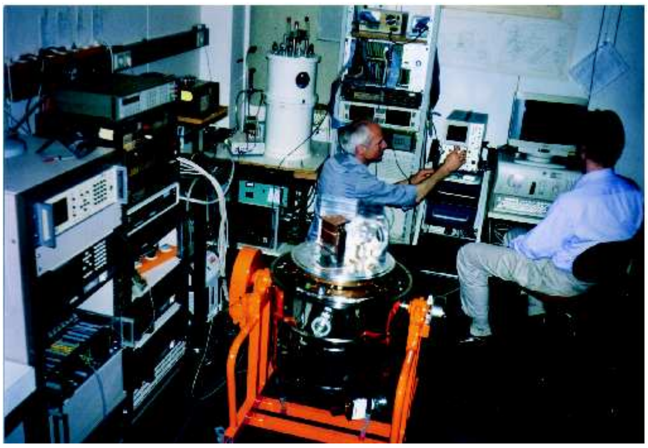

Figure 1. ISOPHOT's subsystems, such as the detector arrays, were characterised in the MPIA infrared laboratory in Heidelberg. A larger cryostat is seen in the foreground centre.

Figure 2. The instrument level tests were performed in the Calibration Facility CALFAC set up in a DORNIER clean room at Friedrichshafen. On the left is the Black Body, in the centre the cryostat housing ISOPHOT, and at the top the liquid helium filling tubes.

to operate Ge:Ga at 3 K and the tight coupling of stressed Ge:Ga to $T < 1.8$ K.

The characterisation of the newly developed CMOS preamplifier/multiplexers (IMEC) operated at 3 K was the second largest task. Although exhibiting some non-ideal characteristics such as debiasing effects, the devices proved to behave reproducibly and were therefore considered calibratable.

The temporal radiation damage caused by ionising particle hits in the Earth's radiation belts was simulated by a radioactive ^{137}Cs source (Figure 3), depositing a similar dose and having similar spike rates to those of ISO's passage (Roth 1994, Schubert et al. 1994). The resulting strong increase in noise, dark current and also responsivity was cured by combinations of bias and temperature increase and infrared flashes from the internal thermal radiation sources (TRS). Given the limitations in heat dissipation and the need for quick temperature stabilisation of the detectors, the IR flashes turned out to be the most effective curing procedure, in particular for the FIR sensors (see Figure 4, and Wilke et al., this volume). Based on these subsystem tests an in-orbit curing procedure for all detector assemblies was developed. Activated after the radiation belts passage this 62 step procedure was applied with only small in-flight modifications at the start of the science window of each orbit (Figure 5) throughout the whole mission.

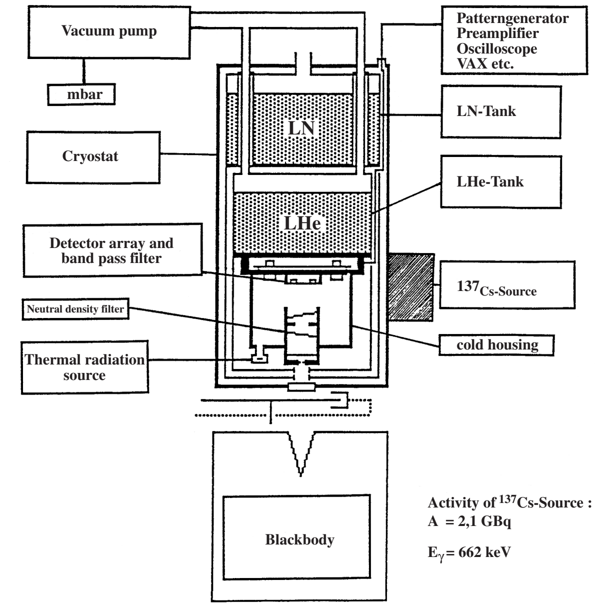

Figure 3. Laboratory set-up for irradiation tests of ISOPHOT's detectors with radioactive sources, simulating the passage of ISO through the Earth's radiation belts.

The instrument-internal thermal radiation sources consisted of small metal coated sapphire wafers which were electrically heated. Two each of these thermal radiation sources (TRS) were combined to form one of two Fine Calibration Sources (FCS) flown with ISOPHOT (see Figure 6). These sources served several purposes: (i) as a flux standard on ISO system level tests and during the early in-orbit phase, (ii) as secondary standards after recalibration on celestial targets and (iii) as flashlights for the detector curing. In laboratory tests the properties of these important devices were studied, such as the wavelength dependent flux vs. electrical heating power and the flux (or temperature) stability of the source.

3. THE CALIBRATION FACILITY (CALFAC)

This facility was developed in order to operate the fully integrated instrument in the simulated ISO environment (Wolf et al. 1993, Wolf et al. 1994). It consisted of three major parts: a large cryostat to house ISOPHOT, beam shaping optics allowing the instrument to be illuminated by an f/15 beam as in the ISO telescope and a Black Body as the standard source (see Figures 7 and 8). The low photon background was achieved by a

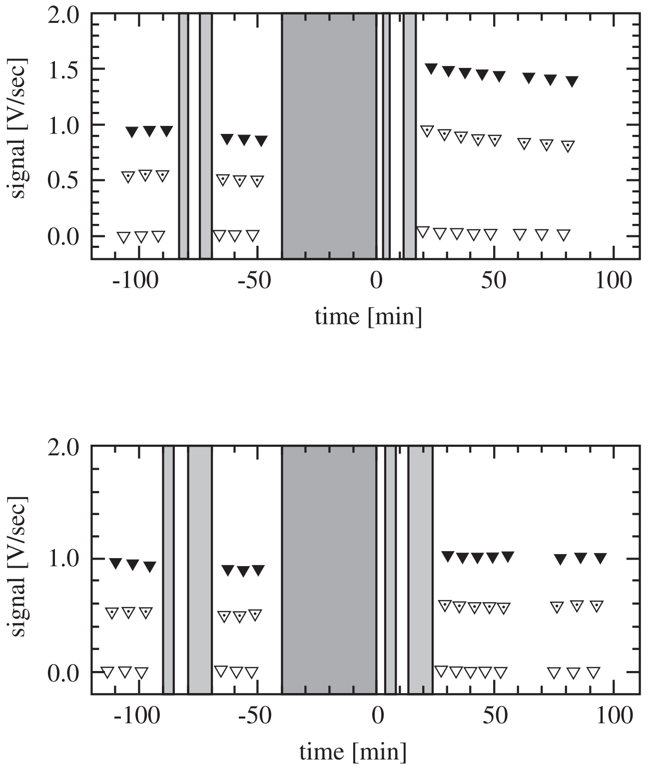

Figure 4. High energy irradiation tests of the stressed Ge:Ga arrays (C200). The dark grey region indicates the irradiation by the ^{137}Cs source (see Figure 3), the light grey regions are flashes by the TRS. Prior to the simulated passage two curings checked the stability of the detector responsivity. In the upper panel the curing by the flashes after passage are not sufficient to heal out the temporary radiation damage, the signals stay high. In the lower panel the duration of the flashes was lengthened and additionally the bias was increased from 80 mV to 120 mV during the first flash. By this the original responsivity of the detectors was re-established within 3 %.

7.1 Sequence for the complete activation of ISOPHOT (switch on and curing of all detectors)

```
================================================================================
PHT - Activation Sequence
-------------------------
All 4 Instruments used in Orbit

Step   Dur.  Description                      TC     TM        Remarks
  #   (sec)
--------------------------------------------------------------------------------
1       0.00 Enable hard and softlimit                          Abort activation
             monitoring for PDU voltage                         if hard limit
             and EEU temperature                                violated
2       2.00 Power on                                prime
3      30.00 On-board software init                  prime
4       0.00 Check parameter M37                     prime
             (self test check)
5       0.00 Check parameter M234 (selftest-ROM)     prime
6       0.00 Check parameter M235 (selftest-RAM)     prime
7       8.82 Initialise Instrument           PF4000  prime
8       9.06 CRE latchup recovery            PF4005  prime
9       0.00 Check parameter M156                    prime     Allow next 30 s
             (CRE SUB+ G1) back to nominal                     for check
10      0.00 Check parameter M157                    prime     Allow next 30 s
             (CRE SUB+ G2) back to nominal                     for check
11      2.00 Temperature control code        PF41    prime
12      2.00 P2-FM default temperature       PF42    prime
13      2.00 P3-FM default temperature       PF43    prime
14      2.00 C100-FM default temperature     PF44    prime
15      2.00 CHW position look-up table      PF45    prime
16      2.00 CHW timing parameter table      PF46    prime
17      2.00 Thermal curing hold time P1     PF47    prime
18      2.00 Thermal curing hold time S1     PF48    prime
19      2.00 Thermal curing hold time S2     PF49    prime
20      2.00 Thermal curing hold time P2     PF50    prime
21      2.00 Chopper parameters (part 1)     PF58    prime
22      2.00 Chopper parameters (part 2)     PF59    prime
23      2.00 Chopper parameters (part 3)     PF60    prime
24      2.00 C200 stand-by bias (part 1)     PF61    prime
25      2.00 C200 stand-by bias (part 2)     PF62    prime
26      2.00 P2 stand-by bias (part 1)       PF63    prime
27      2.00 P2 stand-by bias (part 2)       PF64    prime
28      2.00 P1 stand-by bias                PF65    prime
29      2.00 Ensure CHW emergency current    PF51    prime
30      2.00 CHW safety routine (part 1)     PF52    prime
31      2.00 CHW safety routine (part 2)     PF53    prime
32      2.00 CHW safety routine (part 3)     PF54    prime
33      2.00 CHW safety routine (part 4)     PF55    prime
34      2.00 CHW safety routine (part 5)     PF56    prime
35      2.00 CHW safety routine (part 6)     PF57    prime
36      TBD  Wait for completion of                  prime
             RAM patches
37     20.72 RAM dump (part 1)               PF4001  prime
38     15.34 RAM dump (part 2)               PF4002  prime
39      0.00 Perform RTA/QLA memory check            prime     Allow next 500 s
                                                               for check
40      2.00 Thermal curing of P1            PF4016  prime     ( 281.88 s)
41      2.00 Thermal curing of S1            PF4017  prime     ( 148.88 s)
42      2.00 Thermal curing of S2            PF4018  prime     ( 148.88 s)
43      2.00 Thermal curing of P2            PF4019  prime     ( 69.54 s)
44      2.00 Flash curing of C100 1st        PF4014  prime     ( 149.96 s)
45      2.00 Flash curing of P3   1st        PF4015  prime     ( 158.60 s)
46      2.00 Flash curing of C200 1st        PF4013  prime     ( 279.76 s)
47   1223.50 Wait                                    not prime instr. active
48   >=0.00 Wait (optional)                          not prime instr. inactive
-- -- -- -- -- -- -- -- -- -- -- -- -- -- -- -- -- -- --

49      2.00 Flash curing of C100 2nd        PF4028  prime     ( 277.60 s)
50      2.00 Flash curing of P3   2nd        PF4029  prime     ( 286.24 s)
51      2.00 Flash curing of C200 2nd        PF4027  prime     ( 534.32 s)
52   1092.16 Wait                                    not prime instr. active
53   >=0.00 Wait (optional)                          not prime instr. inactive
-- -- -- -- -- -- -- -- -- -- -- -- -- -- -- -- -- -- --

54     63.70 Responsivity check P1           PF4021  prime
55     63.88 Responsivity check P3           PF4022  prime
56     82.22 Responsivity check S1/S2        PF4023  prime
57     55.24 Responsivity check C100         PF4024  prime
58     56.32 Responsivity check C200         PF4025  prime
59     64.42 Responsivity check P2           PF4026  prime
60      0.00 Check P2 latch-up behavior:             prime     >contingency
             Check M156 (CRE SUB+ G1) and                      procedure
             check for noisy ramps

61     34.38 Configure to Reset Mode         PF4030  prime
--------------------------------------------------------------------------------

Total time          : 2891.76 sec = 48.1 min
PHT needed as prime:  576.10 sec =  9.6 min
--------------------------------------------------------------------------------
```

Figure 5. The complete activation sequence for all detectors of ISOPHOT developed during the preflight tests. It was initiated after passage through the radiation belts and used almost unchanged during the whole mission.

combination of cold attenuation filters inside the cryostat. This concept allowed the beam shaping optics to be at room temperature and the use of an accurate laboratory "Black Body" with temperatures of up to $T \leq 900\,K$. The latter had to be "water cooled" because the entire beam was confined to a vacuum. Two different entrance windows of the cryostat had to be used to cover the large wavelength range (KRS-5 for $\lambda < 30\,\mu m$, TPX for $\lambda > 30\,\mu m$). A special valve allowed the change of entrance windows without breaking the cryo-vacuum.

The accuracy of the calibration of detectors and the FCS in the CALFAC was limited by the following factors:

- The flux from the Black Body was known to within a few percent only.
- The transmission of the spectral filters was determined to within a few percent.
- The transmission of the chain of several attenuation filters was known to an accuracy of $\pm 30\,\%$. This rather large margin of error was caused by wavelength dependent deviations of the transmission from the idealised "neutral density" (Figure 9), and by reflections between several of these filters, although they were tilted.

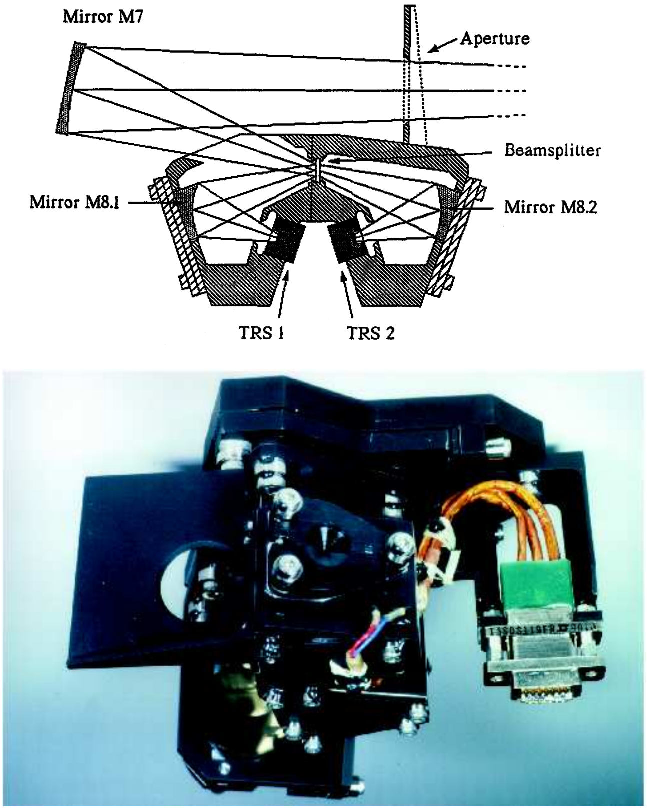

Figure 6. One Fine Calibration Source (FCS) consists of two Thermal Radiation Sources (TRS). By means of a coated diamond beam splitter the fluxes of TRS 1 and TRS 2 were made different by 3 orders of magnitude.

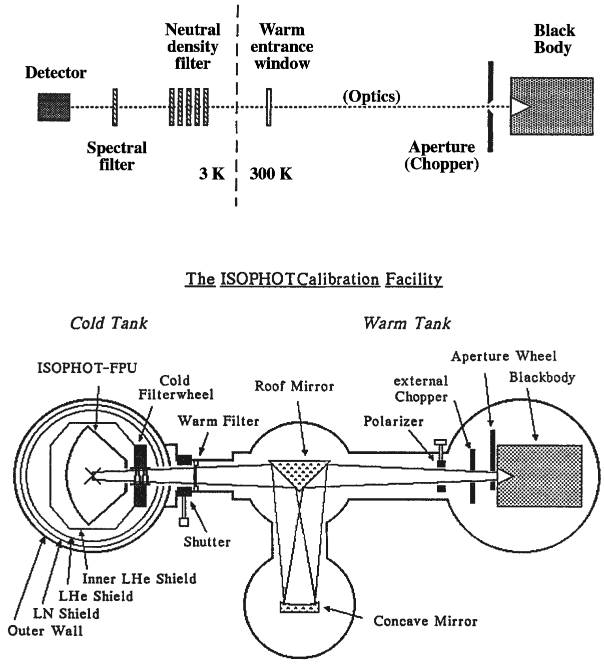

Figure 7. Simplified scheme for the ISOPHOT instrument calibration in the Calibration Facility (CALFAC).

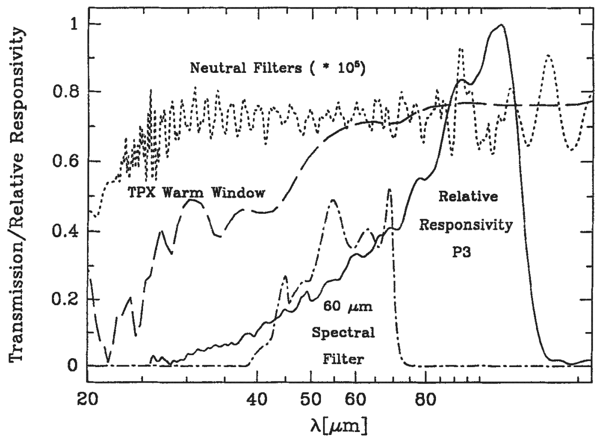

Figure 9. The flux onto the detectors is influenced by the complex transmission curves of several components in the beam.

– 300 K straylight from the rim of the elliptical beam shaping mirror accepted by the slightly oversized focal plan chopper.
– Transmission and emission of the cryostat's entrance window were known to within a few percent.
– Finally, uncertainties such as the spatial angle and geometrical effects such as diffraction added another $\pm 10\,\%$ estimated error.

In summary, we calculated systematic errors of up to $\pm 40\,\%$ as the uncertainty of this preflight calibration. This was sufficient to characterise the instrument fully and set all initial operational parameters. The in-flight calibration on celestial targets was considered to be the final basis of the scientific operation.

For reasons of budget and time, we developed a comprehensive standard test procedure allowing all ISOPHOT modes to be characterised within two working days. The scheme of this test is given in Fig. 10; it is self-explanatory. A change of the entrance window of the cryostat was required between the "long" and the "short" wavelength tests. These extensive standard tests were performed several times in exactly the same manner and therefore allowed the reproducibility of the instrument to be determined. The high reproducibility actually achieved was very satisfying. As one example, the flux sequence of step 8.2 of the C200 photometry (see Figure 10) is given in Figure 11. The signals measured on 10 March 1994 agree within 1 % with those registered in the same test on 22 February 1994 on pixel 1,1 of the C200 camera at $\lambda \sim 180\,\mu$m. This example is typical for the high reproducibility achieved in all channels.

The last sections of the preflight tests in the CALFAC were devoted to a study of the various Astronomical Observing Templates (AOTs). In order to allow the applicability of special observing modes, the Black Body section was equipped with po-

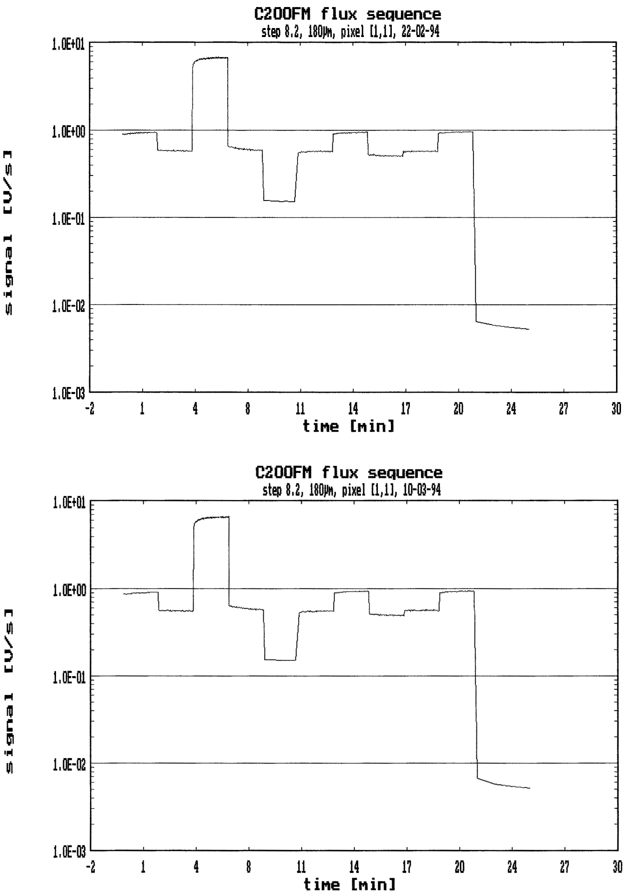

Figure 11. The same flux sequence (step 8.2 of Figure 10) applied to the C200 camera (pixel 1,1 shown) on 22 February and 10 March 1994 resulted in the same signals, demonstrating the reproducibility. This is a precondition for an accurate calibration in flight.

larisers, a chopper, an aperture wheel to simulate stars and extended objects and even a rotating spiral mask to simulate the slews of the Serendipity Survey. These tests revealed that due to detector transients longer observing times would be required than those theoretically derived from the measured NEPs of the detectors. No irradiation tests with ionising particles simulating the Earth's radiation belts were allowed in the CALFAC located in DORNIER's cleanroom.

4. FLIGHT MODEL OR FLIGHT SPARE?

The performance of the flight model (FM) as well as that of the flight spare (FS) derived from the preflight calibration are documented in Tables 1 and 2, respectively. While the differences in the performance of the far infrared channels are balanced between both units, there is a big difference in the Noise Equivalent Power (NEP) of the MIR detectors P1 and P2. The much higher sensitivity (lower NEP) achieved in the FS unit is due to the last minute installation of BIB detectors, whereas the FM is equipped with the original bulk Si:Ga and Si:B detectors (Wolf et al. 1995). As a consequence, the FS was delivered to ESA for integration into the ISO cryostat. During cold tests of the ISO payload, however, the filter wheels of the ISOPHOT-FS occasionally showed incorrect positioning. This was diagnosed as increased friction in the ball bearings, in particular of wheel 3. The reopening of the cryostat for other reasons provided the opportunity to exchange the FS unit by the FM. The much preferred repair of the BIB detector equipped FS unit and the subsequent requalification would have required a few weeks, much longer than the short window allowed for the exchange.

5. PREDICTING THE "IN-FLIGHT PERFORMANCE"

The results of the ground calibration in the CALFAC were combined with data from ISO's telescope to predict the in-flight performance as the basis for the initial observing proposals. For ISOPHOT's broad band filters in the MIR and FIR and its rather large diffraction limited beams another factor comes into play: brightness and structure of the celestial background. The wavelength region 10 to 60 μm is dominated by the thermal emission of the interplanetary dust (IR zodiacal light), while the FIR sky is dominated by the emission of interstellar dust (cirrus) with the maximum brightness in the 100 to 200 μm range. While the zodiacal light is structureless and distributed regularly, the cirrus has a patchy structure on all angular scales and can vary greatly on the arcmin scale. This latter effect contributes to the "confusion noise" in the FIR, a limit only avoided with larger size telescopes.

The predicted performance is compared in Table 3 with the one measured in-flight on celestial standard stars. The values differ typically by a factor of 2, somewhat more on the P3 Ge:Ga detector, due to a higher dark current encountered in-flight. Most detectors are limited, as expected, by the natural sky emission. Given the necessarily incomplete ground calibration (without telescope, satellite, radiation belts, etc.) the agreement between "predicted" and "measured" is satisfactory. This is particularly true for the at that time unknown territory, the wavelength region 110 to 240 μm.

6. TESTING AFTER INSTRUMENT DELIVERY

With the instrument delivery to ESA 16 months before launch, the characterisation and calibration did not stop. It was even continued during the early part of the mission. Using replica detectors almost identical to those in the instrument, a few non-ideal properties could be studied in detail and corrective measures developed.

One of the newly developed cold-readout electronics (CRE) occasionally exhibited a "soft latch-up" effect, resulting in a higher supply current and increased noise. By optimising the switch-on sequence of the supply voltages for the CRE, the latch-ups could be avoided. One CRE developed this effect during the mission and again the parallel laboratory work helped to find a method of cancellation.

The Si:Ga detectors operated with a high bias voltage ($\leq$ 90 V) were required to be illuminated with fluxes of

$< 10^{-12}$ W, in order to avoid break-through and protect the CRE input. When this restriction led to operational overheads (screening, monitoring) early in the mission, laboratory tests on the corresponding replica detectors resulted in a relaxation of this flux limit.

A reduced responsivity was observed for the single P detectors as compared to earlier laboratory tests of the corresponding detector materials. A destructive disintegration of one replica detector revealed an insufficient cavity as the reason for the signal loss. It contained too much absorbing surface (glue, sapphire) and was not polished enough by the manufacturers.

The signal transients for the Si:Ga detectors were theoretically modelled and the model refined by corresponding laboratory measurements (Figure 12). This work was mostly performed by J. Schubert (MPIA) and our guest B. Fouks and finally honoured by the Fouks-Schubert formula used in data reduction of several ISO instruments nowadays (Schubert et al. 1995).

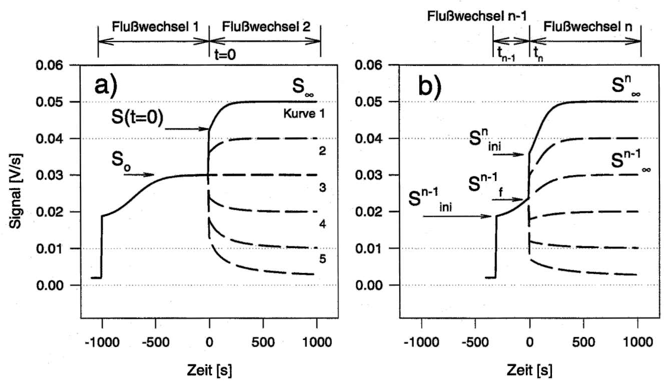

Figure 12. Signal behaviour of the Si:Ga detectors (PHT-S) derived for a sequence of flux changes (Flußwechsel) plotted vs. Time (Zeit). Taken from J. Schubert's thesis (MPIA/Univ. Heidelberg) which forms the basis of the widely used Fouks-Schubert formula.

The CALFAC containing the ISOPHOT-FS model was held in stand-by during the early part of the mission. In case of failures of the flight unit, in particular of the cryomechanisms, the trouble could have been simulated and counter measures developed. Fortunately all wheels and the chopper showed excellent performance during the long mission, so the stand-by FS never had to be activated.

7. SUMMARY

The preflight calibration achieved optimal settings for the operational parameters of the instrument and a reasonable sensitivity prediction for the mission. It gave us full confidence in the reproducibility of all the measurements and on the reliability of its operation. It allowed the establishment of the "in-orbit" calibration requirements and the successful commissioning of the instrument.

Difficulties later encountered in space were identified on ground. For the elimination of most radiation induced effects in the detectors, curing methods were developed preflight and applied in-orbit. Soft latch-up effects in CREs and transient effects of several detectors had corrective methods developed before launch.

It was a useful approach to extensively characterise subsystems such as detectors in the laboratory and consequently limit the more demanding instrument calibration in the CALFAC to a period of a few weeks. It was also reasonable to restrict the effort for the preflight calibration accuracy to about 40 %, because this allowed all goals to be achieved and the mission to depend on the continuous in-flight calibration.

Having two instruments, the FM and the FS, turned out to be useful this time, because we were able to exchange them once. However, this requires "Go/No-go" criteria to be established early in the development. From a PI point of view the repair of a failed instrument, although requiring a greater time interval for a replacement, is certainly less costly. Finally, using replica detectors to continue the characterisation after the instrument delivery turned out to be highly productive. If an FS instrument is available, it should be in standby for simulations of trouble experienced on board and to effectively and safely develop counter-procedures.

ACKNOWLEDGEMENTS

This work was supported by the Max Planck Society and funds from the DLR (formerly DARA), Bonn. The contributions by the Danish Space Research Institute, Lyngby, which delivered the Electrical Ground Support Equipment and by the Instituto de Astrofisica de Canarias, La Laguna, which characterised the spectrophotometer PHT-S are particularly acknowledged. Dr. E. Popow from the Astrophysikalisches Institut Potsdam supported us during the peak calibration period. We also enjoyed the support of the DORNIER and ZEISS industrial teams during this period, as well as that of ESA's ISO Project Team. The authors take sole responsibility for this report.

REFERENCES

Grözinger, U., Kirches, S., Lemke, D. et al., 1993, ESA SP-256, 329

Laureijs, R.J., Klaas, U., Richards, P. et al., 2000, The ISO Handbook, Volume V: PHT – The Imaging Photo-Polarimeter, SAI/99-069/Dc, Version 1.1, November 1, 2000, Villafranca

Lemke, D., Lützow-Wentzky, P., Fricke, W. et al., 1993, Cryogenics 33, 395

Lemke, D., Garzón, F., Gemünd, H.P. et al., 1993, SPIE 2019, 28

Roth, G., 1994, Diplomarbeit, Univ. Heidelberg

Schubert, J., Roth, G., Wolf, J. et al., 1994, SPIE 2268, 28

Schubert, J., Lemke, D., Fouks, B., 1995, SPIE, 2553, 461

Wilke, B., Grözinger, U., Klaas, U., Lemke, D., 2003, this volume

Wolf, J., Gabriel, C., Grözinger, U. et al., 1993, SPIE 2019, 82

Wolf, J., Gabriel, C., Grözinger, U. et al., 1994, Opt. Engineering 33, 26

Wolf, J., Wiest, L., Grözinger, U. et al., 1995, SPIE 2553, 482

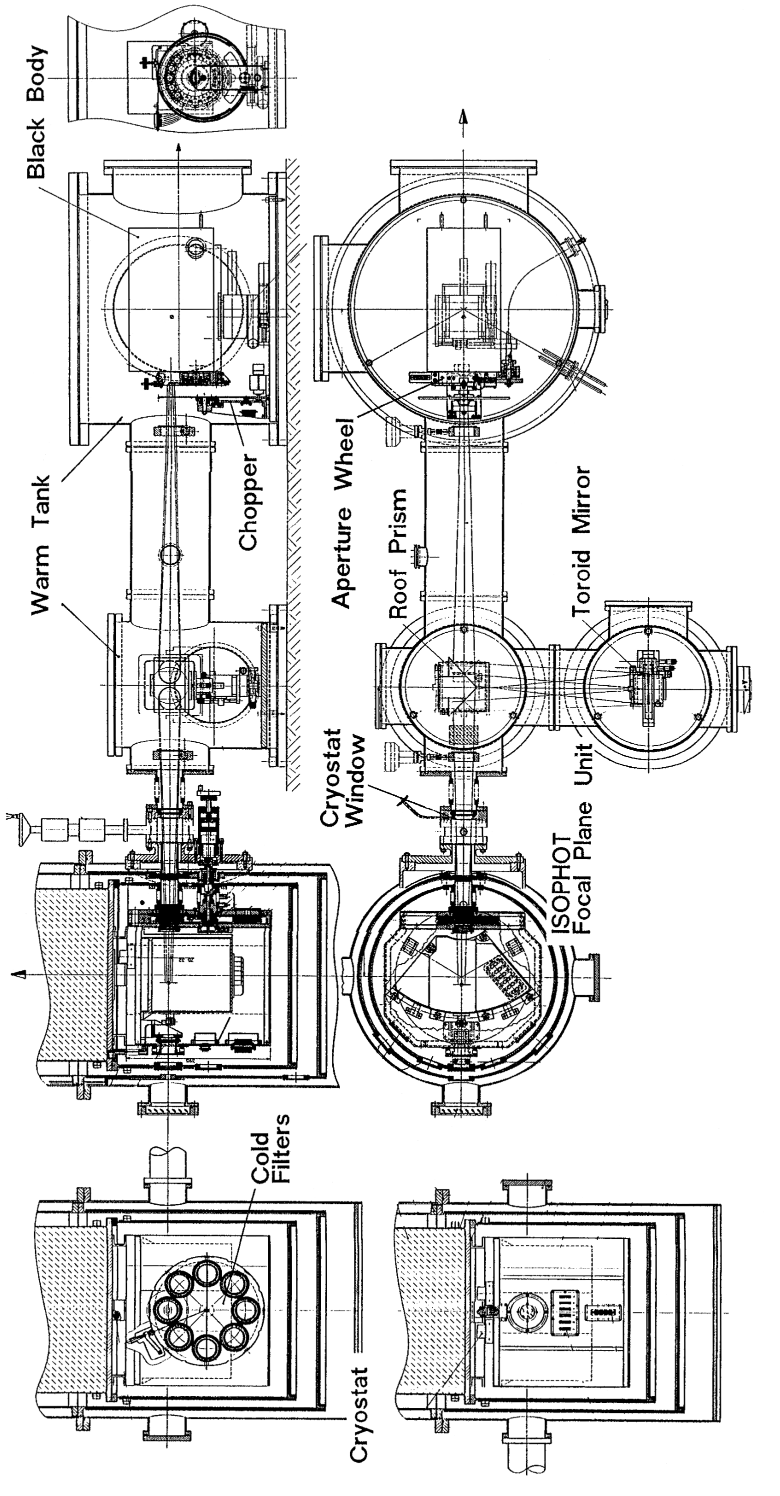

Figure 8. The CALFAC; see also Figure 7. On the left is the cryostat with several onion-shell-arranged cold housings guaranteeing the very low radiation background. In the centre are the beam shaping optics simulating ISO's f/15 beam. To the right is the Black Body with aperture/polariser wheel and a rotating chopper in front of its cavity.

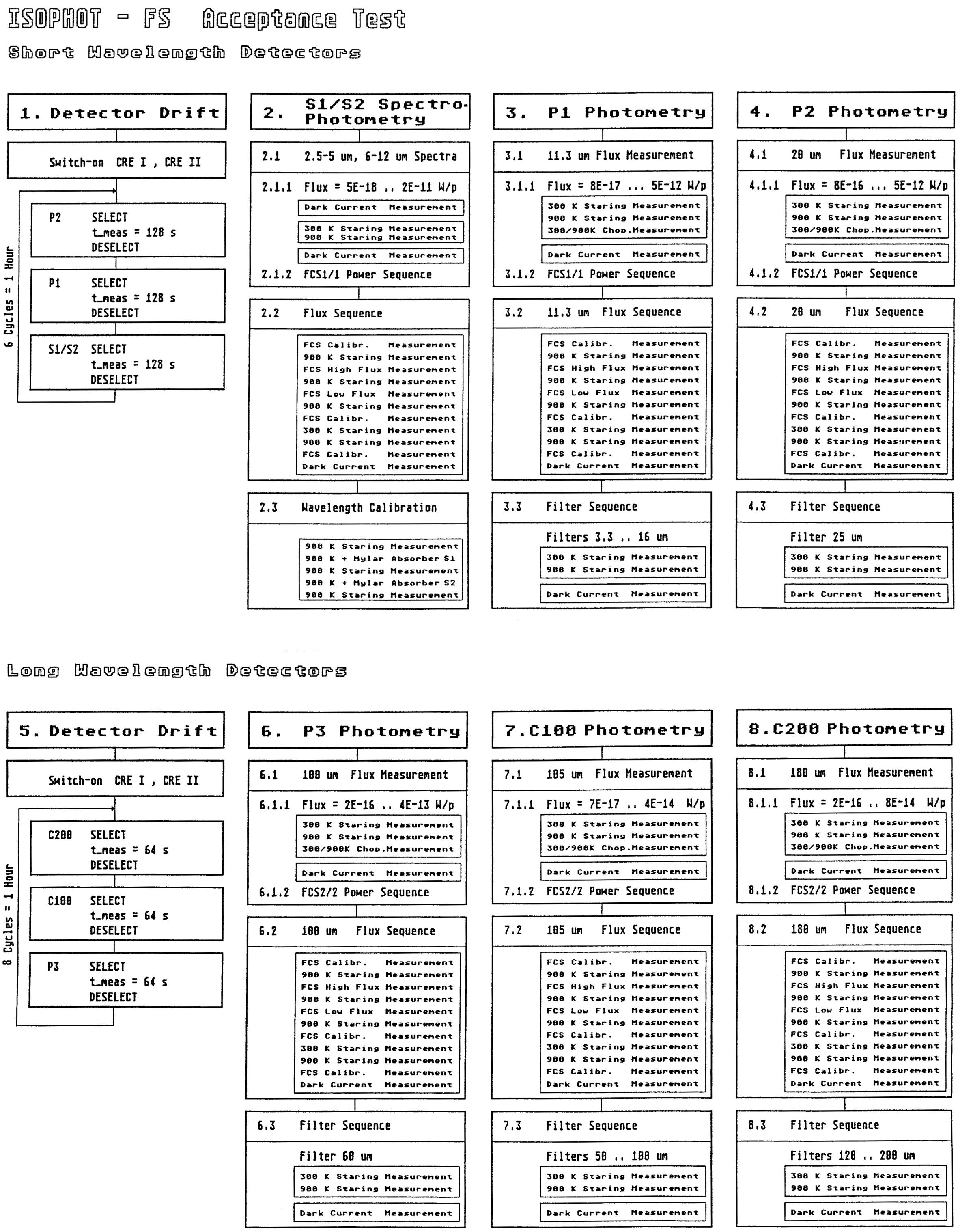

Figure 10. The standard tests allowed the full characterisation of the instrument in all channels within 2 days. Between the two test blocks (short λ, long λ) the entrance window of the cryostat was changed from KRS-5 to TPX. The repetition of these tests within weeks allowed the long term reproducibility of ISOPHOT to be confirmed.

Table 1. ISOPHOT-FM Performance Data derived from acceptance test AT1-FMup of 22/24-Feb-1994 in the CALFAC.

Detector	$\lambda_{\max}$ [μm]	T [K]	Bias [V]	900K-Flux [W/pixel]	R [A/W] measured	NEP [W/$\sqrt{Hz}$] measured	η	G	NEP_{det} [W/$\sqrt{Hz}$] ([1])	Dark current [e/s]
PHT-P1	15	2.9	90	$1.3 \cdot 10^{-15}$	0.59	$1.5 \cdot 10^{-16}$	0.004	11.8	$1.6 \cdot 10^{-16}$	1595
PHT-P2	25	3.6	10	$4.8 \cdot 10^{-15}$	0.67	$1.5 \cdot 10^{-16}$	0.015	2.2	$2.2 \cdot 10^{-16}$	3825
PHT-P3	100	2.8	0.250	$5.9 \cdot 10^{-16}$	17.4	$2.0 \cdot 10^{-17}$	0.084	2.6	$3.5 \cdot 10^{-18}$	123
PHT-C100	100	3.0	0.180	$2.3 \cdot 10^{-16}$	29.0	$1.4 \cdot 10^{-17}$	0.135	2.7	$8.7 \cdot 10^{-18}$	7471[2]
PHT-C200	180	1.8	0.080	$4.3 \cdot 10^{-16}$	14.7	$1.0 \cdot 10^{-17}$	0.144	0.7	$1.2 \cdot 10^{-17}$	1869
PHT-S2	15	2.9	37	$2.0 \cdot 10^{-16}$	0.4–1.3	$4.0 \cdot 10^{-17}$	0.030[3]	1.7	$3.1 \cdot 10^{-17}$	< 1000
PHT-S1	15	3.0	37	$2.0 \cdot 10^{-16}$	1.6–3.1	$3.0 \cdot 10^{-17}$	0.210[4]	0.7	$1.3 \cdot 10^{-17}$	< 600

[1]) = minimum achievable NEP using noise of lowest measured dark current
[2]) = without pixel [1,2], dark signal is a factor of 10 higher than mean
[3]) = calculated as mean over λ = 2.5 ... 5 μm
[4]) = calculated as mean over λ = 5 ... 12 μm

Table 2. ISOPHOT-FS Performance Data derived from acceptance test AT1-94 & AT2-94 of 26-Oct/25-Nov-1994 in the CALFAC.

Detector	$\lambda_{\max}$ [μm]	T [K]	Bias [V]	900K-Flux [W/pixel]	R [A/W] measured	NEP [W/$\sqrt{Hz}$] measured	η	G	NEP_{det} [W/$\sqrt{Hz}$] ([1])	Dark current [e/s]
PHT-P1	23	2.9	3.5	$1.9 \cdot 10^{-16}$	23.0	$4.8 \cdot 10^{-18}$	0.173	7.3	$4.5 \cdot 10^{-18}$	553
PHT-P2	23	3.6	3.5	$1.4 \cdot 10^{-15}$	36.0	$2.3 \cdot 10^{-17}$	0.277	7.1	$5.1 \cdot 10^{-18}$	1072
PHT-P3	100	2.8	0.250	$5.9 \cdot 10^{-16}$	10.9	$1.3 \cdot 10^{-17}$	0.093	1.5	$6.4 \cdot 10^{-18}$	246
PHT-C100	100	3.0	0.180	$2.1 \cdot 10^{-16}$	38.2	$1.5 \cdot 10^{-17}$	0.166	2.9	$6.3 \cdot 10^{-18}$	7133[2]
PHT-C200	180	1.8	0.080[3]	$4.3 \cdot 10^{-16}$	10.4	$1.0 \cdot 10^{-17}$	0.144	0.5	$3.8 \cdot 10^{-18}$	4342
PHT-S2	15	2.9	37							
PHT-S1	15	3.0	37							

[1]) = minimum achievable NEP using noise of lowest measured dark current
[2]) = without pixel [1,3], [2,1] and [2,3]; mean dark signal of all pixels is factor 1.9 higher
[3]) = individual bias voltages: [1,1] = 76 mV, [1,2] = 73 mW, [2,1] = 81 mW, [2,2] = 77 mW
PHT-S data evaluation ongoing; sensitivities probably unchanged.

Table 3. Predictions for the in-flight performance are derived from the preflight calibration and compared to the performance actually achieved during the mission (taken from ISO Handbook, Vol. 5, Table 2.1, Laureijs, Klaas et al. 2000): ISOPHOT Sensitivity Limits: S/N = 1, 256 s on-source integration time, 1 reference background position. The numbers in parentheses in the "Pre-flight" column give an estimate of the 1 σ confusion noise at the corresponding background brightness. The confusion noise has to be added to the pure detector noise limit. The in-flight values include all possible noise sources.

Detector	Filter	Aperture [arcsec]	Sensitivity Pre-flight [mJy]	In-flight [mJy]	Background [MJy sr^{-1}]	Limiting Parameter
P1	P_4.85	52 circ.	2	2.5	0.1	detector noise
P1	P_11.5	52 circ.	2	5	15	background noise (ZL)
P2	P_25	79 circ.	7	13	40	background noise (ZL)
P3	P_60	180 circ.	3.5(+5)	20	10	detector/cirrus noise dark current 100× higher
C100	C_90	45 (1 pix)	1(+5)	7.5	10	detector/cirrus noise
C200	C_160	90 (1 pix)	3(+21)	40	5	cirrus noise
S1(SL)		24 × 24	21	10	15	detector/background noise
S2(SS)		24 × 24	11	26	0.5	detector noise